AIAA–2002–2948

Active Flow Control to Improve the Aerodynamic and Acoustic Performance of Axial Turbomachines

Lars Neuhaus and Wolfgang Neise
DLR
Berlin, Germany

1st Flow Control Conference
24 – 27 June 2002
St. Louis, Missouri

ACTIVE FLOW CONTROL TO IMPROVE THE AERODYNAMIC AND ACOUSTIC PERFORMANCE OF AXIAL TURBOMACHINES

L. Neuhaus and W. Neise

Deutsches Zentrum für Luft- und Raumfahrt e.V., Institut für Antriebstechnik, Abteilung Turbulenzforschung, Müller-Breslau-Str. 8, 10623 Berlin, Germany

Abstract

The tip clearance flow of axial turbomachines is important for their aerodynamic and acoustic performance. The rotating instability phenomena and the tip clearance noise are observed on axial turbomachines with significant tip clearance. Previous investigations show that it is possible to reduce the tip clearance noise and improve the aerodynamic performance of the fan by mounting a turbulence generator into the tip clearance gap. In this paper it is shown that these improvements can be obtained without any modification of the tip clearance gap itself by actively controlling the tip clearance flow. To achieve this, air is injected into the gap through slit nozzles mounted flush with the inner casing wall.

With steady air injection it is possible to obtain – with a small injected mass flow – a remarkable reduction of the noise level along with an improved aerodynamic performance. With larger injected mass flows, significant improvements of the aerodynamic performance are obtained at the expense of a steep increase of the noise level.

Unsteady air injection synchronized with the impeller rotation yields a significant improvement of the aerodynamic performance accompanied by a substantial increase of the noise level. Rotating instability and tip clearance noise can be reduced in both cases.

Flow investigations with a simplified stationary 2D blade cascade show that steady air injection leads to a diminished blade tip vortex and with it to an improved aerodynamic performance.

1. INTRODUCTION

Axial turbomachines have a radial gap between the casing and the rotor blades. The static pressure difference between the suction and the pressure side of impeller blades produces a secondary flow over the tip of the rotor blades (Figure 1). This tip clearance flow is important for the aerodynamic and acoustic performance of the machine. The pressure rise and efficiency drop and the usable range of the performance characteristic is diminished as the rotor flow is stalled at higher flow rates.

Previous work at DLR-Berlin [1]-[4] investigating the effects of varying tip clearances on noise and performance showed the existence of a broad-band noise source for large tip-casing clearances. This source appeared in the rotor wall pressure spectrum at about half the blade passing frequency (BPF) and radiated a fluctuating tonal component into the far field, the tip clearance noise (TCN). Interpretation of the spectra and circumferential mode analyses led to the model of a rotating source mechanism, called rotating instability (RI), which moves relative to the blade row at a fraction of the shaft speed, similar to the cells of rotating stall (Kameier [1], Kameier and Neise [2]). The effect was also observed in the third stage of the low-speed research compressor at the TU Dresden when the tip clearance was enlarged (Müller and Mailach [5]).

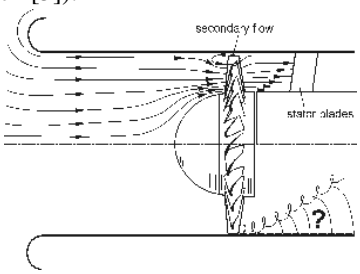

Figure 1: Schematic view of the secondary flow driven by the pressure difference between the suction and pressure side in the tip region.

Kameier [1] was successful in reducing the tip clearance noise and to increase the aerodynamic performance by mounting a turbulence generator into the tip clearance gap (see also Kameier and Neise [3]), compare Figure 2. The aim of the present work is to reproduce and possibly improve the effect achieved with the turbulence generator without modifications of the tip clearance gap itself to make the method applicable also to flow machines where the tip clearance gap is changed, e.g., due to usage of different stagger angles of the impeller blades.

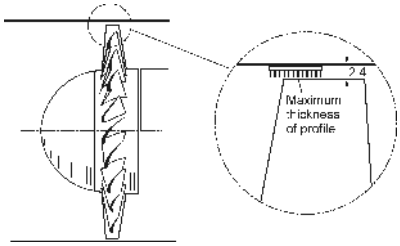

Figure 2: Schematic view of the tip clearance gap with the turbulence generator inserted.

The investigation is supported by the German National Science Foundation as part of the "Sonderforschungsbereich 557, Beeinflussung komplexer turbulenter Scherströmungen" conducted at the Technical University of Berlin.

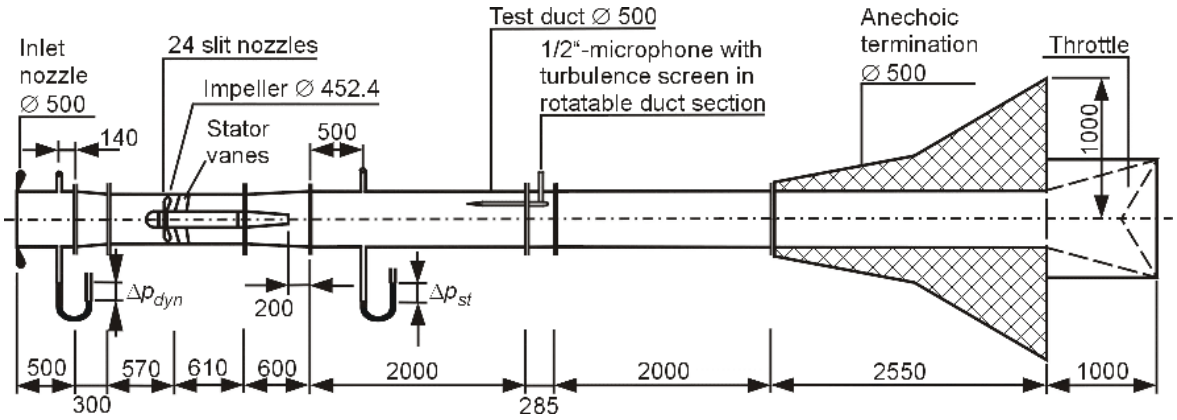

Figure 3: Experimental setup (dimensions in mm).

2. EXPERIMENTAL FACILITY

The test fan is a low-speed high-pressure axial fan with outlet guide vanes, the same as used for the experiments [1], [2] and [3]. The principal impeller dimensions are as follows: impeller diameter D = 452,4 mm; hub-to-tip ratio $\varepsilon = 0.62$; NACA 65 blade profile; blade number $Z = 24$; blade chord length at the tip $c = 43$ mm; maximum bade thickness 3 mm; blade stagger angle at the tip $\theta = 27°$. The design speed is $n = 3000$/min. The stator row comprises V = 17 unprofiled vanes. The axial distance between rotor and stator at the outer circumference is $\Delta x/c = 1.3$. The tip clearance can be varied by exchanging casing segments while the impeller diameter remains constant. Four casing segments are available to give the following tip clearances: s = 0.3, 0.6, 1.2, and 2.4 mm ($\zeta = s/c$ = 0.7%, 1.4%, 2.8%, and 5.6%). All experiments reported here were made with the 2.4 mm wide tip clearance gap ($\zeta = s/c$ =5.6%).

Figure 3 shows the experimental setup with its major dimensions. The measurement facility is in accordance with the requirements of DIN 24136 [6] for measurement of aerodynamic fan performance. On the inlet side there is a short duct section with a bellmouth nozzle; there are no flow straighteners or screens in the inlet duct. The anechoically terminated outlet duct is in accordance with the international standard ISO/FDIS 5136 [7].

In the outlet duct a ½-inch microphone equipped with a turbulence screen is mounted in a rotatable duct section to measure the circumferentially averaged sound pressure level at a specified radial distance from the duct axis. To measure the unsteady blade pressure, a miniature pressure sensor is mounted on the suction side of one impeller blade at 36% of the chord length without changing the original outer blade contour. The radial distance from the blade tip is 7% of the chord length.

To control the flow conditions in the tip clearance gap, air is injected into the gap through slit nozzles mounted flush with the inner casing wall, as is shown in Figure 4. The axial position of the slit of the nozzles is 0.3 mm upstream of the impeller blades. The nozzles can be placed at up to $Z_{noz} = 24$ uniformly distributed circumferential positions. The angle between the jet axis and the interior casing wall is 15°. The slit nozzles are pivoted in the casing wall so that the angle between the main flow direction and the jets can be varied within 360°. The air flow of the injection is controlled by electronic proportional directional valves with a usable frequency range up to 200 Hz.

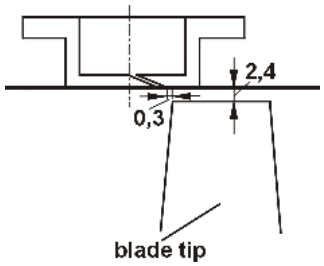

Figure 4: Schematic view of a slit nozzle.

3. FLOW CONTROL WITH STEADY AIR INJECTION

3.1 Experiments with Z = 24 jet nozzles

The first experiments were conducted with steady air injection using $Z_{noz} = Z = 24$ nozzles which is equal to the number of impeller blades. Measurements were made at two impeller speeds, the design speed $n = 3000$/min and at $n = 600$/min.

Figure 5 shows the aerodynamic and acoustic performance curves for the design speed $n = 3000$/min. For symbols and the definitions of the non-dimensional fan performance parameters used, see the appendix. The injected mass flow is given in percent of the maximum mass flow delivered by the fan (i.e., at φ = 0.3). Incidentally, at the injected mass flow rate of $m_{in} = 0.8\%$, the jet flow velocity amounts to Ma = 0.18. With steady air injection, pressure rise and efficiency increase at low flow rates, and the stall point is shifted towards lower flow rates.

With the mass flow injection rates of 0.6% and 0.8%, the optimum efficiency is increased, and with the largest rate of 1% the maximum efficiency is decreased slightly.

The sound pressure characteristic without air injection exhibits the occurrence of tip clearance noise at operating points near $\varphi = 0.2$. When the injected mass flow is raised up to 0.8%, the sound pressure level is lower over the whole range of the performance characteristics. When the injected air flow is increased further (m_{in} = 1%), the sound pressure level becomes higher than without air injection, except for those operating points where tip clearance noise exists.

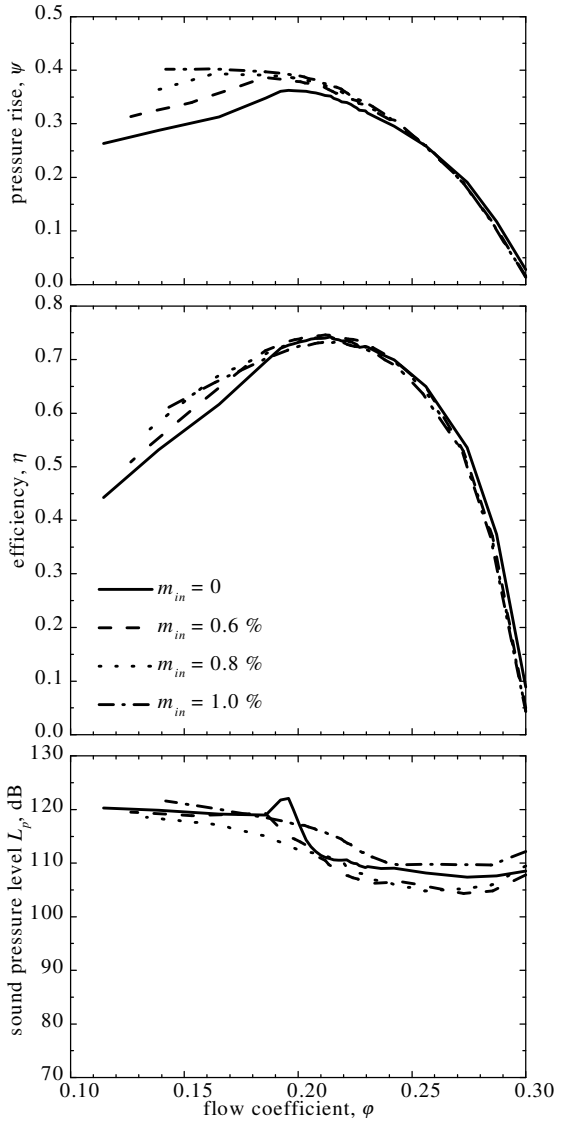

Figure 5: Pressure coefficient, efficiency, and sound pressure in the outlet duct as functions of the flow coefficient for different steady air injection mass flows; n = 3000/min, Z_{noz} = 24, ζ = 5.6%.

Figure 6 shows sound power spectra in the fan outlet duct and wall pressure spectra on the suction side of one impeller blade. When the injected air flow is lower than m_{in} = 0.8%, rotating instability (RI) is visible in the blade wall pressure spectrum and tip clearance noise (TCN) in the sound pressure spectrum. When the injected mass flow rates is 0.8%, RI and TCN disappear.

The level of the blade passing frequency (BPF) is found to increase with the injected air flow which is due to the interaction between the jets from the nozzles and the impeller blades. Despite the increase in BPF-level, the overall sound pressure level is reduced, e.g., at m_{in} = 0.8% from 123 dB to 113 dB, where the BPF level increases from 101 dB to 109 dB.

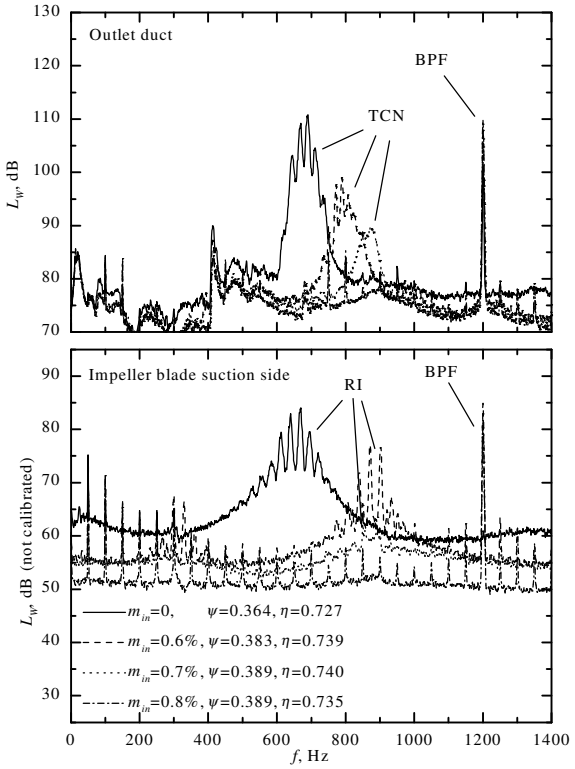

Figure 6: Spectra of sound power in the fan outlet duct and wall pressure on the rotor blade suction side for different steady air injection rates; n = 3000/min, Z_{noz} = 24, ζ = 5.6%, φ = 0.2.

The changes in fan pressure and efficiency due to the air injection are given in the legend of Figure 6.

Tests with steady air injection were also made at a fan speed of n = 600/min which is much lower than the design speed to enable a direct comparison with the later experiments with unsteady injection (see Chapter 4) where the pulse frequencies are to be synchronized with the blade passing frequency. As mentioned before, the maximum operating frequency of the valves is 200 Hz which limits the speed of the impeller for these tests.

Figure 7 shows the influence of steady air injection on the aerodynamic and acoustic fan performance at this low impeller speed. At low flow coefficients and high injection rates, the fan pressure is improved by as much as 55% and no blade flow stall is visible in the fan characteristics (m_{in} = 1.7%). The measured improvement of the fan efficiency is even larger, up to 53%, however, this result has to be taken with a grain of salt because of the way the efficiency is determined here, i.e. the ratio of fan aerodynamic

power to the sum of the electric power input to the drive motor plus the aerodynamic power of the injected air flow (compare the definition given in the appendix). At low rotational speeds, the electric efficiency of the drive motor is very low which in turn makes the measured approximate fan efficiency also very low with a probable large measurement uncertainty because of the temperature dependence of the electric efficiency. For this reason, the efficiency improvements documented in Figure 8 have to judged with caution.

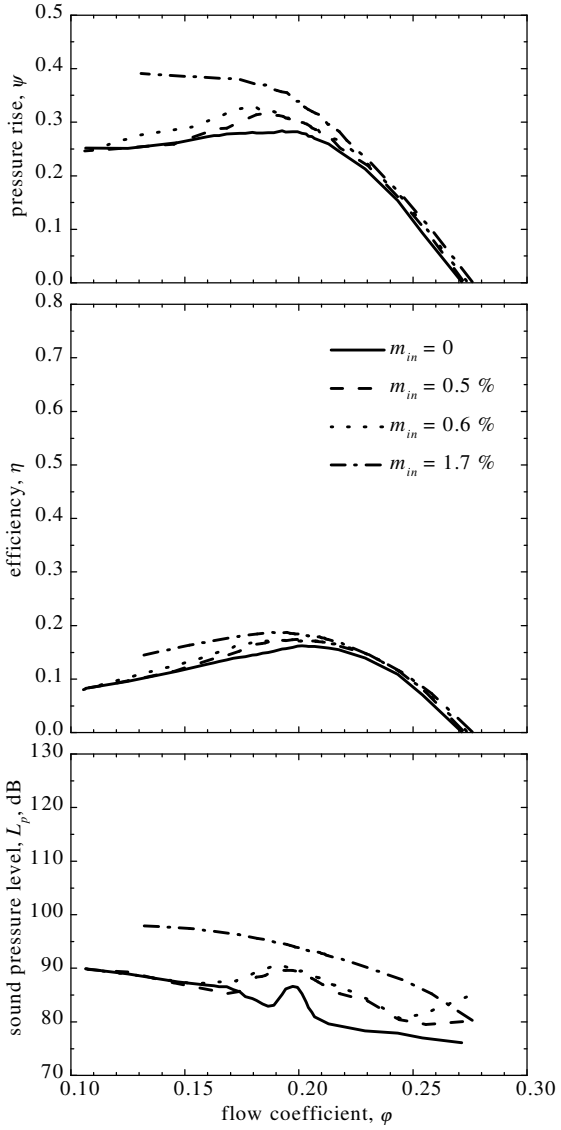

Figure 7: Pressure coefficient, efficiency, and sound pressure in the outlet duct as functions of the flow coefficient for different steady injection mass flows; n = 600/min, Z_{noz} = 24, ζ = 5.6%.

At the low impeller speed, the overall sound pressure level in the outlet duct is higher than without air injection until the flow gets stalled. The reason for that can be explained with the help of Figure 8. Without air injection, the BPF-level in the outlet duct is very low because the rotor/stator interaction as the main cause of this tone component generates a spinning mode of the order $m = 7$ ($V = 17$, compare Tyler and Sofrin [8]) which is not propagational in the outlet duct. The mode caused by the interaction between the injected jets and the impeller blades is the $m = 0$ ($Z = Z_{noz} = 24$). This is the plane wave mode which is cut on at all frequencies, and thus the BPF-level increases when the air is injected. The spectra in the outlet duct and on the suction side of one impeller blade (Figure 8), show that RI and TCN begin to disappear at an injected mass flow of $m_{in} = 0.6$ with a jet velocity of $Ma = 0.023$. In conclusion, it is possible to suppress RI and TCN at this low impeller speed but there is no improvement in the overall noise level because of the increased blade tone level.

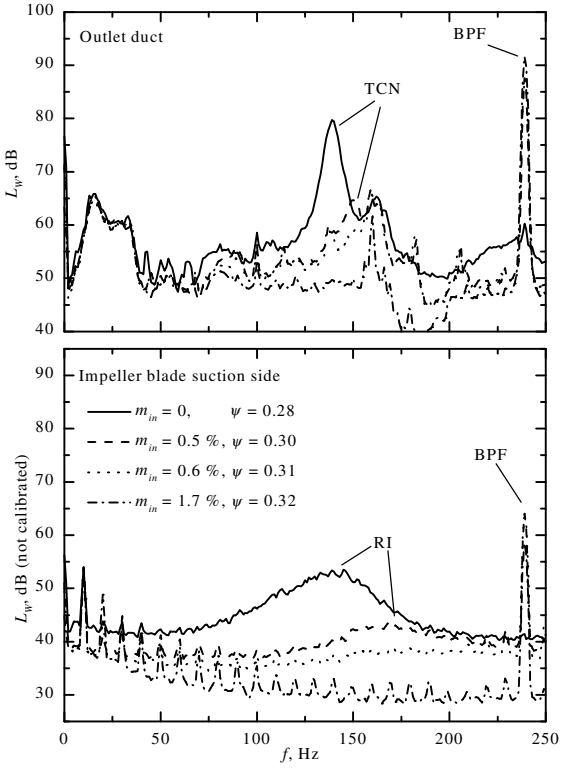

Figure 8: Spectra of sound power in the fan outlet duct and wall pressure on the rotor blade suction side for different steady air injection rates; n = 600/min, Z_{noz} = 24, ζ = 5.6%, φ = 0.2.

3.2 Experiments with Z_{noz} = 12 jet nozzles

To demonstrate the influence of the number of injection nozzles, Figure 9 shows the aerodynamic and acoustic fan performance curves when only Z_{noz} = 12 evenly distributed jet nozzles are used. As in the case with Z_{noz} = 24 (compare Figure 5), fan pressure and efficiency increase at low flow rates when steady air injection is applied. The stall point in the case Z_{noz} = 12 and m_{in} = 0.4% is nearly the same as in the case Z_{noz} = 24 and m_{in} = 0.8%. The optimum efficiency is improved slightly at small air injection rates and somewhat impaired at higher rates. This loss in optimum efficiency is larger for Z_{noz} = 12 than for Z_{noz} = 24.

The acoustic fan performance is improved over the whole range of flow coefficients for injection rates below or equal to m_{in} = 0.4%.

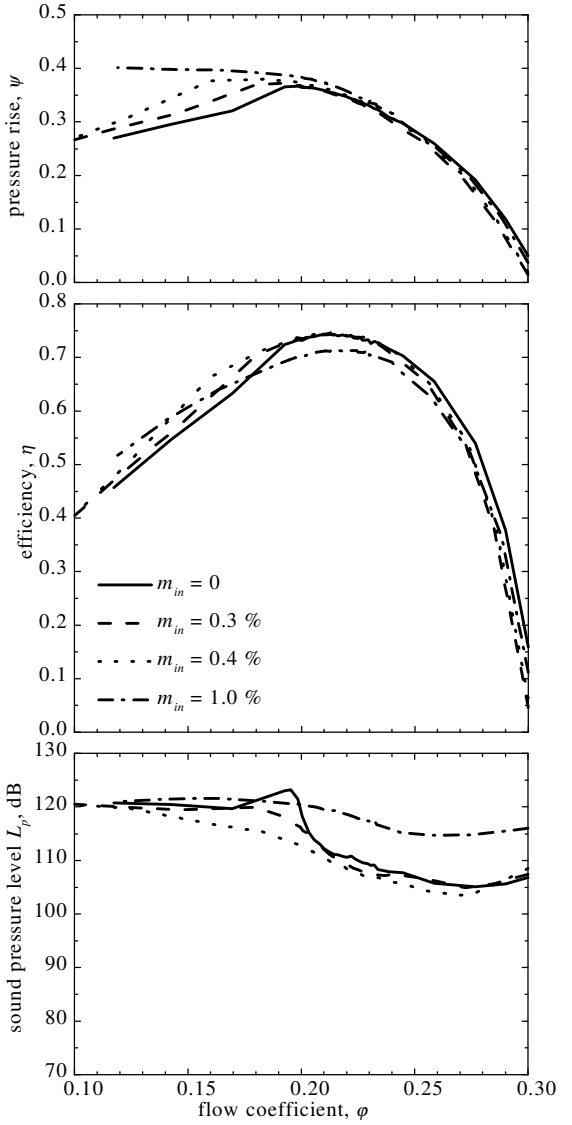

Figure 9: Pressure coefficient, efficiency, and sound pressure in the outlet duct as functions of the flow coefficient for different steady air injection mass flows; n = 3000/min, Z_{noz} = 12, ζ = 5.6%.

The corresponding spectra of sound power in the fan outlet duct and suction side blade wall pressure spectra are shown in Figure 10 for the operating point $\varphi = 0.2$. RI and TCN are completely suppressed when the injected mass flow is $m_{in} = 0.4\%$ or higher. At $m_{in} = 0.4\%$, the BPF-level is increased from 101 dB to 105 dB, nevertheless the overall level is reduced by about 10 dB down to 113 dB. Further increasing the injected air flow leads to higher BPF-levels and, in turn, to smaller reductions of the overall level.

In the blade wall pressure spectra a peak appears at half the blade passing frequency, which is the "jet passing" frequency sensed by the rotating impeller blades.

Comparing the results with 12 and 24 nozzles leads to the conclusion that the injected mass flow which is needed for the complete suppression of RI and TCN is reduced by 50% when only half as many nozzles are used. In both cases the velocity of the injected air is the same, $Ma = 0.18$.

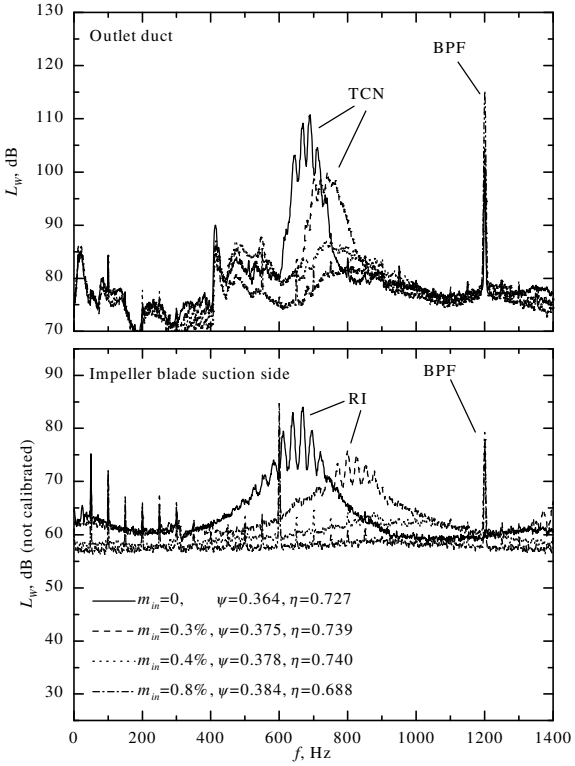

Figure 10: Spectra of sound power in the fan outlet duct and wall pressure on the rotor blade suction side for different steady air injection rates; n = 3000/min, Z_{noz} = 12, ζ = 5.6%, φ = 0.2

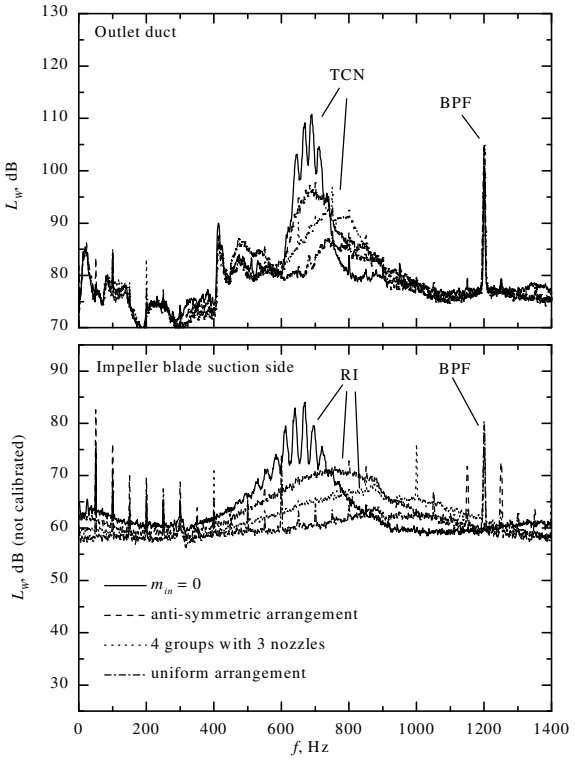

Figure 11: Spectra of sound power in the fan outlet duct and wall pressure on the rotor blade suction side for steady air injection ($m_{in} = 0.4\%$) and different

circumferential nozzle configurations; n = 3000/min, Z_{noz} = 12, ζ = 5.6%, φ = 0.2

3.3 Experiments with uneven distributions of jet nozzles

Figure 11 shows the sound power spectra in the outlet duct and the blade wall pressure spectra obtained with three different circumferential arrangements of Z_{noz} = 12 jet nozzles which are sketched in Figure 12. The fan operation point is $\varphi = 0.2$ and the injected mass flow rate is $m_{in} = 0.4\%$. Complete suppression of RI and TCN is only reached with the uniform nozzle arrangement. With the other two arrangements it is also possible to reduce RI and TCN but only at the expense of a higher broadband noise level. The BPF-level is not affected by the circumferential nozzle arrangement. Increasing the injected mass flow even further does not influence RI and TCN.

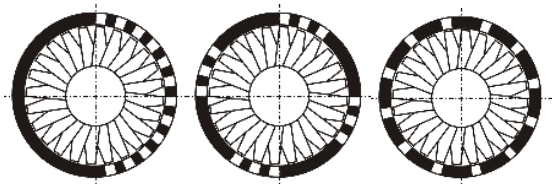

Figure 12: Sketch of the circumferential nozzle configurations; a) anti-symmetric arrangement; b) 4 groups with 3 nozzles; c) uniform arrangement.

4. FLOW CONTROL WITH UNSTEADY AIR INJECTION

As mentioned before in chapter 2, proportional directional valves were used for the experiments with unsteady air injection. Up to frequencies of f_{in} = 200 Hz the mass flow passing the valves oscillates nearly sinusoidally. Tests were made with n = 600/min impeller speed where the blade passing frequency is 240 Hz. The injection frequency was selected to be one-half of the BPF. The electric drive signal of the valves was synchronized with the impeller rotation. Because of the limited frequency range of the valves it is not possible to match injection frequency with the blade passing frequency. Tests at lower rotational speeds are not possible either because RI does not exist any more.

The unsteady mass flow rate can not be measured and set directly, the following steps are necessary instead: First the valves are fully opened, and the injected mass flow is adjusted to a certain required value. Then the unsteady valve operation is turned on which results in a time averaged mass flow which is equal to one half of the previously set flow rate with the valves fully open.

Figure 13 shows aerodynamic and acoustic fan performance curves with unsteady air injection. As before with steady injection, fan pressure and efficiency at low flow rates are increased; the higher the injected flow rate, the more the stall point is shifted to lower flow rates.

Different from the results with steady injection, the overall sound pressure level is always higher than without air injection. When the injected mass flow is increased to $m_{in} = 0.88\%$ the sound pressure level in the outlet duct is nearly constant over the whole range of flow coefficients. This shows that the noise caused by the pulsating jets is much higher than the fan noise, dominating the overall sound pressure level.

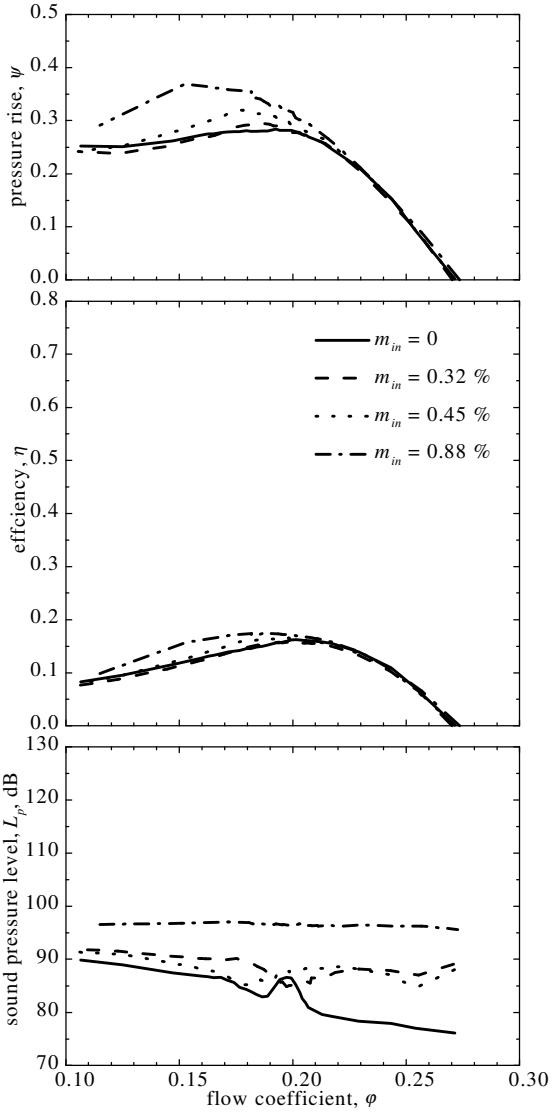

Figure 13: Pressure coefficient, efficiency, and sound pressure in the outlet duct as functions of the flow coefficient for different unsteady air injection rates; n = 600/min, Z_{noz} = 24, f_{in} = 120 Hz, ζ = 5.6%.

The corresponding sound power spectra in the outlet duct and the blade suction side wall pressure spectra are shown in Figure 14 for the flow coefficient $\varphi = 0.2$. RI and TCN disappear when the injected mass flow is equal to or higher than $m_{in} = 0.45\%$. Similarly to the steady air injection, the BPF-level increases due to the interaction between the jets and the impeller blades. To reduce this interaction, it would be desirable to set the phase of the air

injection such that the jets are blown into the blade channel between two subsequent blades. This however is not possible because of the limited frequency range of the valves. In addition to the BPF-peak, another tonal component appears in the sound pressure spectra at the injection frequency f_{in} = 120 Hz. At high flow injection rates (m_{in} = 0.88%), the blade wall pressure spectra are dominated by peaks at the rotor frequency and its harmonics. These pressure fluctuations appear only in the source region and are not radiated into the outlet duct.

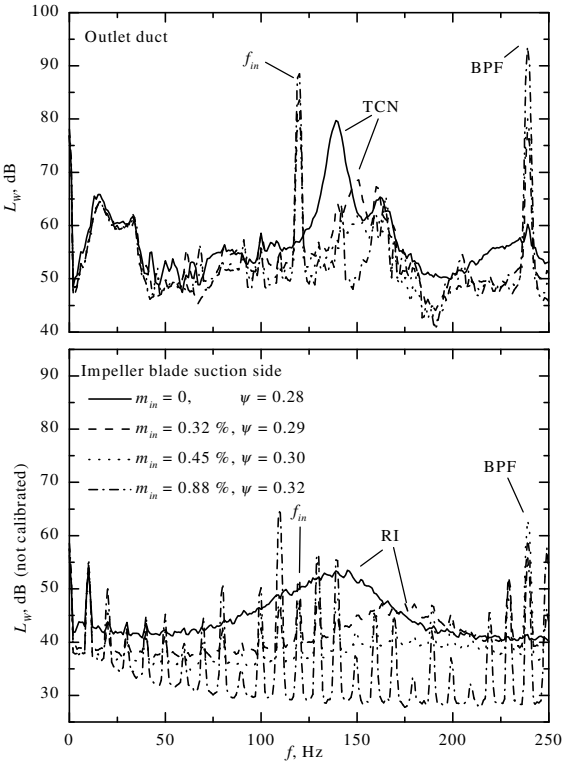

Figure 14: Spectra of sound power in the outlet duct and blade suction side wall pressure with unsteady air injection; n = 600/min, Z_{noz} = 24, f_{in} = 120 Hz, ζ = 5.6%, φ = 0.2

5. COMPARISON BETWEEN STEADY AND UNSTEADY AIR INJECTION

In Figure 15 results obtained with steady and unsteady air injection are compared. The injected mass flow rate is m_{in} = 0.4%. Two cases of unsteady injection are considered, both at one-half of the blade passing frequency but with and without sychronization with the impeller rotation.

With unsteady air injection, the improvements in the pressure coefficient at low flow rates are better than with steady injection with regard to both shifting the stall point to lower flow rates and increasing the fan pressure. There is hardly any difference between the cases where the flow injection is synchronized with the impeller rotation and where it is not.

To improve the fan efficiency at optimum operation and higher volume flows, steady air injection is better suited than the unsteady one. The opposite is true for operating points to the left of the point of optimum operation. Again, there is no difference between the results for synchronized and unsynchronized injection.

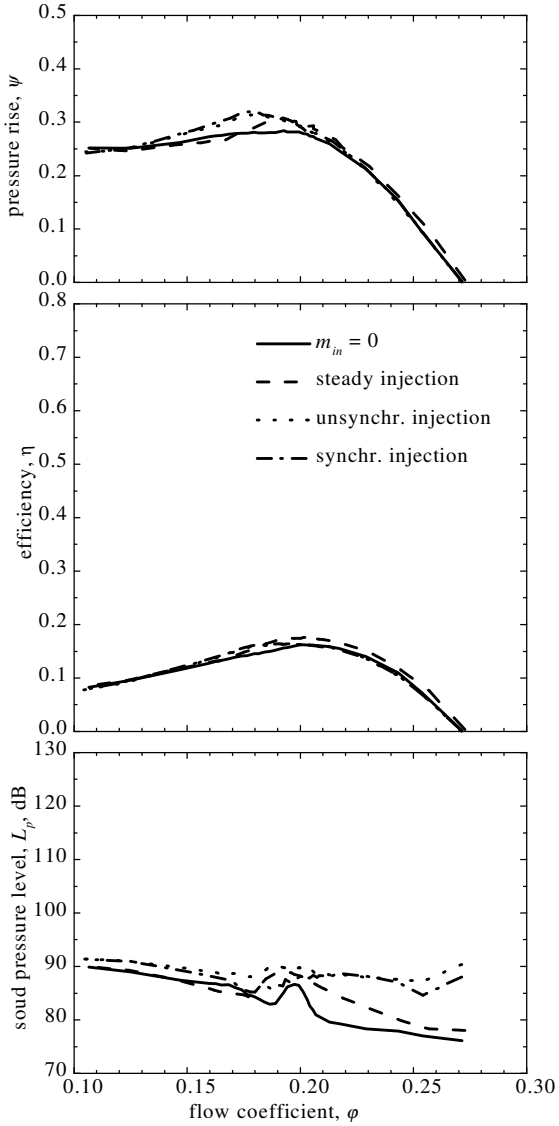

Figure 15: Pressure coefficient, efficiency, and sound pressure in the outlet duct as functions of the flow coefficient for steady and unsteady air injection; n = 600/min, Z_{noz} = 24, ζ = 5.6%, m_{in} = 0.45%

Both steady and unsteady flow injection lead to higher sound pressure levels. The reason for that is given in the previous chapter. The levels observed with synchronization are lower than without.

Inspecting the spectra plotted in Figure 16 shows that RI as well as TCN can be eliminated by applying unsteady air injection. Steady injection at the rate m_{in} = 0.45% reduces RI and TCN, but does not completely suppress these spectral components.

The increases in BPF-level due to unsteady flow injection are higher without than with synchronization. Also, without synchronization higher levels at the pulse frequency are observed.

The BPF level with steady air injection is higher than with synchronized unsteady air injection which

is due to the fact that in this case each impeller blade is hit by a jet when passing by while in the unsteady excitation at 0.5·BPF this is true for only every other blade.

When the unsteady air injection is not synchronized with the impeller rotation, slight variations of the rotor speed lead to changing coincidences of blades and jets so that on average each blade interacts with the air jets, and as a result, the BPF-level is higher than with synchronization.

More details on the unsteady injection with and without synchronization are given by Neuhaus et. al. [9], Schulz et. al. [10], and Schönbeck [11].

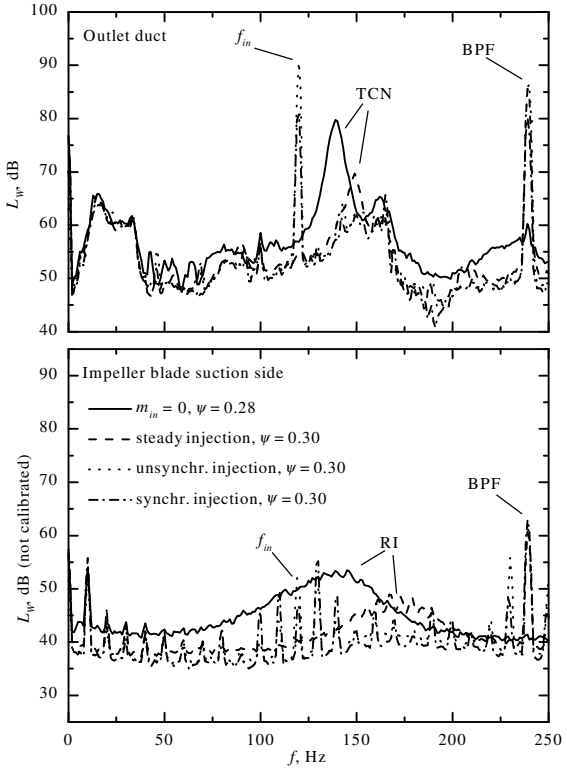

Figure 16: Spectra of sound power in the fan outlet duct and wall pressure on the rotor blade suction side for steady and unsteady air injection; n = 600/min, Z_{noz} = 24, m_{in} = 0.45%, ζ = 5.6%, φ = 0.2.

6. FLOW INVESTIGATION ON STATIONARY BLADE CASCADE

To obtain a better understanding of the physical mechanisms involved in the interaction of the air injected through the nozzles with the rotor blade flow, flow visualization and PIV experiments were made with a simplified two-dimensional cascade model in a wind tunnel, see the principal sketch in Figure 17. The study was carried out by Fuchs [12] in the context of her diploma thesis. Here, sample results of the investigation are presented.

The model experiment was designed to match the flow conditions of the experimental fan as closely as possible. The cascade consisted of 3 blades with a cord length of c_{mod} = 100 mm. The tip clearance ratio ζ = 0,56% is the same as in the experimental fan. The Reynolds number of the cascade flow is nearly equal to that of the rotor tip flow at the impeller speed n = 600/min. The angle of attack of the airfoils was set to match the flow conditions of the impeller blades for the operating point φ = 0.2. The velocity of the wind tunnel flow is 6.4 m/s.

The slit nozzles used for the cascade experiments are the same as in the test fan because had they been scaled up with the blade dimensions, they would have been quite large and would have blocked too much of the optical window available for the PIV-experiments. Hence, the momentum of the air injection in the cascade experiments is smaller than in case of the fan experiments. The axial position of the slit of the nozzles is 0.6 mm upstream of the airfoils, and the velocity of the injection is Ma = 0.015.

The flow around the center airfoil of the cascade is studied using the digital PIV technique. Two optical windows are employed: The first is parallel with the main flow direction at 10 mm distance from the blade tip, and the other is located at the trailing edge of the airfoil perpendicular to the main flow direction, compare Figure 17.

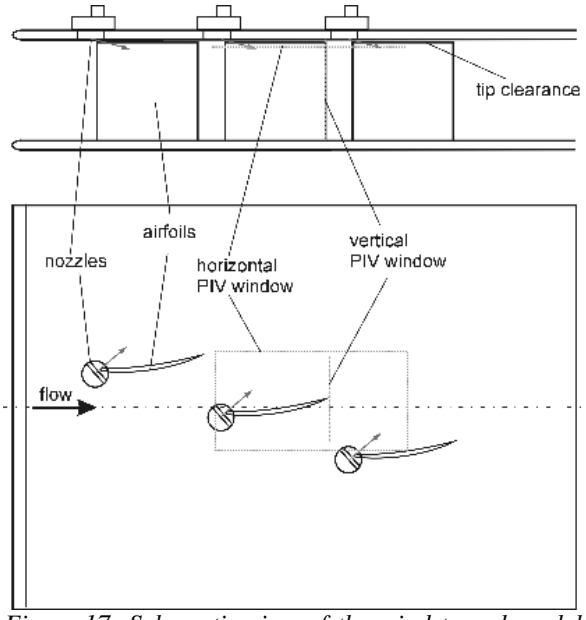

Figure 17: Schematic view of the wind tunnel model with the horizontal (dotted) and vertical (dashed) PIV window

Figure 18 and Figure 19 show the flow field without and with air injection, respectively. The grey areas in the flow field were not accessible optically for the PIV-analysis because of shadows etc. The airfoil is printed in white. Even though the momentum of the air injection in the cascade experiments is smaller than in case of the fan experiments, the influence of the air injection is clearly visible.

In the case without injection (Figure 18), there is a large region (marked "a") on the suction side of the airfoil where the flow velocity is higher than the main flow velocity of the wind tunnel flow (note that the

wind tunnel speed of 6.4 m/s is indicated by the dark gray color). The two regions (marked “b”) indicate areas with very low velocity. These two regions represent sections through the cores of two different blade tip vortices. The blade tip vortex located on the suction side of the center airfoil is caused by the airfoil itself. The other located on the pressure side of the center airfoil is caused by the neighbor blade of the cascade which is not visible in the picture.

The case with air injection is shown in Figure 19. The flow on the suction side of the airfoil is accelerated more than without air injection. The core of the blade tip vortex moves slightly upwards in the figure. As a result, the distance between the blade tip vortex and the lower the airfoil (not visible in the picture) is slightly larger than without air injection. This can be interpreted as an aerodynamic decoupling of the blades of the cascade.

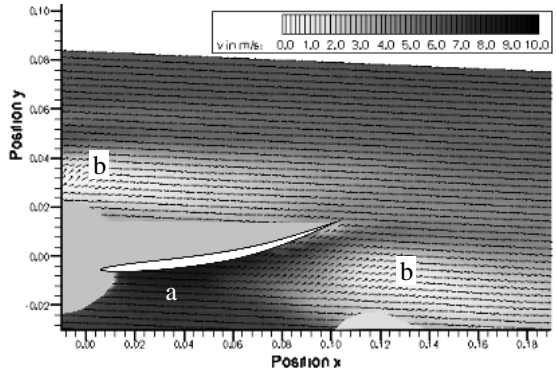

Figure 18: Flow around the center airfoil 10 mm away from the blade tip with no air injection (horizontal PIV window)

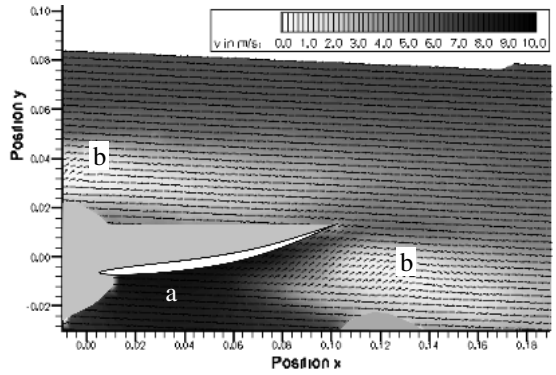

Figure 19 Flow around the center airfoil 10 mm away from the blade tip with air injection (horizontal PIV window)

The results obtained with the vertical PIV windows for the cases without and with air injection are shown in Figure 20 and Figure 21 as streamline plots at the trailing edge of the center airfoil. In both figures are to be seen the core of the blade tip vortex of the center airfoil (region marked "a") and a large region of flow circulation (region marked "b") which encompasses the blade tip vortex of the 1st and the 2nd (center) airfoil. With air injection, the core of the blade tip vortex (a) moves slightly towards center blade of the cascade. This observation supports the above notion of aerodynamic decoupling of the blade flows. Additionally, the circulation region (b) is smaller with air injection than without. This is due to the fact that the circulation of the vortex must maintain constant and the injected mass flow mixes with the vortex. As a result, the flow regime not directly affected by the tip clearance flow, which reaches from the bottom of the airfoil up to the circulation region (b), is larger with air injection and therefore, the aerodynamic performance of the cascade flow is enhanced. Similar reasoning holds for the blade flow of the experimental fan.

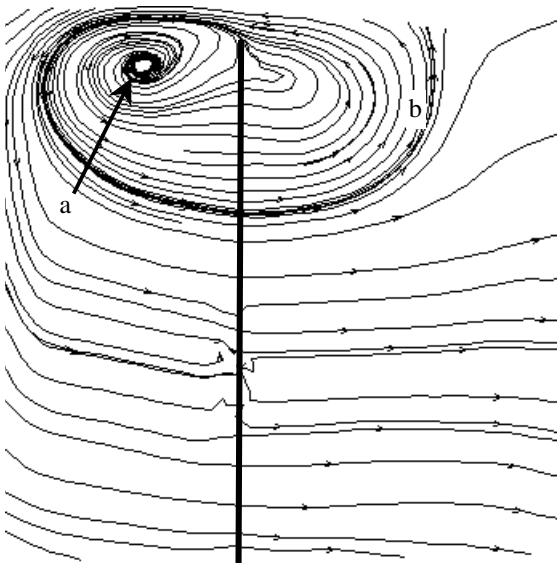

Figure 20: Streamlines at the trailing edge of the blade with undisturbed blade tip vortex

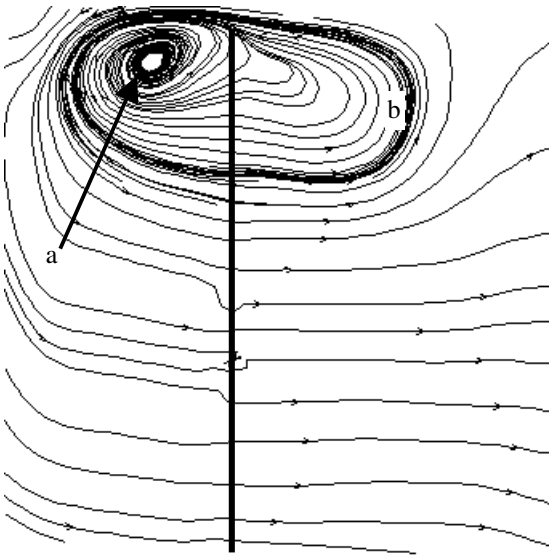

Figure 21: Streamlines at the trailing edge of the blade with disturbed blade tip vortex

7. CONCLUSIONS

Improvements of the aerodynamic and acoustic performance of axial turbomachines can be obtained

with steady or unsteady air injection into the tip clearance gap between the impeller blades and the fan casing. Slit nozzles mounted flush with the inner casing wall are used for the present experiments.

With steady air injection it is possible to achieve – with small injected mass flow rates – a significant reduction of the radiated noise level together with small improvements of the aerodynamic performance or – with high injected mass flow rates – significant improvements of the aerodynamic performance at the expense of a strong increase of the radiated noise level.

Rotating blade flow instability and tip clearance noise disappear from the spectrum when steady air injection is applied.

In the present experiments, the number of injection nozzles used was equal to the impeller blade number or half of it. Best results were obtained with uniform circumferential distributions.

For the fan design speed $n = 3000$/min the required injection velocity is $Ma = 0.18$, and for a reduced speed of $n = 600$/min it is $Ma = 0.023$. The necessary velocity does not scale linearly with the rotor speed or the flow velocity in the fan duct.

Unsteady air injection synchronized with the impeller rotation improves both the pressure coefficient and the fan efficiency at operating points below the optimum which is similar to the effect of steady air injection. This positive aerodynamic result is accompanied by a substantial increase of the blade passage frequency level and the appearance of another tone component at the injection frequency, resulting in a much higher level of the overall radiated sound pressure. Rotating blade flow instability and tip clearance noise are eliminated when the injected mass flow is $m_{in} = 0.45\%$.

The comparison of steady and unsteady air injection shows that the latter is more suitable to improve the fan pressure and to suppress rotating instability and tip clearance noise with lower mass flow injection rates, while steady injection is more effective in enhancing the fan efficiency. Tests with unsteady flow injection could be made only at reduced fan speeds because of the limited frequency range of operation of the unsteady valves used. It is not possible to decide on the basis of the present results if steady or unsteady flow injection is preferable with respect to the overall noise at typical impeller speeds.

It is believed that the excess blade passage frequency noise observed in the present experiments, which is due to the interaction between the impeller blades and the jets, can be avoided by a continuous circumferential slit arrangement. Future tests will explore this possibility.

Flow investigations with a simplified stationary 2D blade cascade show that steady air injection leads to a diminished blade tip vortex and with it to an improved aerodynamic performance.

8. REFERENCES

[1] Kameier, F.: Experimentelle Untersuchungen zur Entstehung und Minderung des Blattspitzen-Wirbellärms axialer Strömungsmaschinen. PhD-Dissertation, Fortschr.-Ber. VDI Reihe 7 Nr. 243, VDI-Verlag, Düsseldorf (1994).

[2] Kameier, F., Neise, W.: Rotating blade flow instability as a source of noise in axial turbomachines. Journal of Sound and Vibration (1997) 203, 833-853.

[3] Kameier, F., Neise, W.: Experimental study of tip clearance losses and noise in axial turbomachinery and their reduction. ASME Journal of Turbomachinery (1997) 119, 460 – 471.

[4] März, J., Hah, Ch., Neise, W.: An experimental and numerical investigation into the mechanisms of rotating instability. Proceedings of ASME Turbo Expo 2001 June 4-7, 2001. New Orleans, Louisiana, USA, Paper 2001-GT-0536.

[5] R. Müller, R. Mailach: Experimentelle Untersuchungen von Verdichterinstabilitäten am Niedergeschwindigkeitsverdichter Dresden, VDI Berichte 1425, 167 – 176.

[6] DIN 24163: Ventilatoren, Teil 1 - 3 Leistungsmessung. Deutsche Norm, Deutsches Institut für Normung e.V., Berlin (1985).

[7] ISO/FDIS 5136: Acoustics – Determination of sound power radiated into a duct by fan and other air-moving devices – In-duct method (Revision of (ISO 5136:1990). International Organization for Standardization, Geneva (2001).

[8] Tyler J. M., Sofrin T. G.: Axial Flow Compressor Noise Studies. Transactions of the Society of Automotive Engineers 70 (1962), 309-332.

[9] Neuhaus, L., Schönbeck, R., Neise, W.: Aktive Beeinflussung des Betriebsverhaltens und Lärms axialer Turbomaschinen. Turbokompressoren im industriellen Einsatz; Tagung Duisburg 18./19.September 2001 / VDI Gesellschaft Energietechnik. VDI-Berichte 1640; ISBN 3-18-091640-0; VDI-Verlag GmbH; Düsseldorf (2001).

[10] Schulz, J., Schönbeck, R., Neuhaus, L., Neise, W., Möser, M.: Aktive Beeinflussung des Betriebsverhaltens und des Drehklangs axialer Turbomaschinen. Ventilatoren: Entwicklung – Planung – Betrieb; Tagung Braunschweig 20./21. Februar 2001 / VDI Gesellschaft Energietechnik. VDI-Berichte 1519; ISBN3-18-091591-9; VDI-Verlag GmbH; Düsseldorf (2001).

[11] Schönbeck, R. Beeinflussung der Schaufelüberströmung eines Axialventilators durch Einblasen

im Kopfspalt. Diploma Thesis, Technische Universität Berlin (2001).

[12] Fuchs, M., Experimentelle Untersuchung der Schaufelumströmung an einem zweidimensionalen Modell eines axialen Gitters durch Drucklufteinblasung im Bereich der Schaufelspitzen, Diploma Thesis, Technische Universität Berlin (2001).

APPENDIX: SYMBOLS

A	cross sectional area ($A_0 = 1$ m^2)
a_0	speed of sound
c	blade chord
c_{mod}	blade chord of the airfoils of the wind tunnel model
d	duct diameter
D	impeller diameter
f	frequency
L_p	pressure level
L_W	sound power level
m_{in}	injected mass flow in percent of the mass flow delivered by the fan at $\varphi = 0.3$
M_{in}	injected mass flow
Ma	$= u/a_0$; flow Mach number
Ma_0	$= u_0/a_0$; jet exit flow Mach number
n	impeller speed
Δp_{stat}	static fan pressure
Δp_t	total fan pressure ($\Delta p_{t0} = 1$ Pa)
P	sound power
P_{el}	electric power input to drive motor
P_{in}	$= M_{in} \cdot u_{in}^2$ aerodynamic power of injected air flow
s	tip clearance
St	$= fD/U$; Strouhal number
u	flow velocity
U	impeller tip speed
u_{in}	jet exit flow velocity
V	number of stator vanes
Q	volume flow ($Q_0 = 1$ m^3/s)
Z	number of impeller blades
Z_{noz}	number of nozzles
ε	hub-to-tip ratio
ζ	$= s/c$; non-dimensional tip clearance
η_t	$= \Delta p_t \, Q/(P_{el} + P_{in})$ approximate total fan efficiency
θ	blade stagger angle
ρ_0	air density
φ	$= 4Q/(\pi D^2 U)$; flow coefficient
ψ	$= 2\Delta p_t/(\rho_0 U^2)$; pressure coefficient